Stability of magnetic LDH composites used for phosphate recovery

Changyong Lu, Tae-Hyun Kim, Jesper Bendix, Mustapha Abdelmoula, Christian Ruby, Ulla Gro Nielsen, Hans Chr Bruun Hansen

Stability of magnetic LDH composites used for phosphate recovery

Changyong Lu[*§], *Tae-Hyun Kim*[‖], *Jesper Bendix*[‡], *Mustapha Abdelmoula*[†], *Christian Ruby*[†], *Ulla Gro Nielsen*[‖], *Hans Chr. Bruun Hansen*[*§]

[§] University of Copenhagen, Faculty of Science, Department of Plant and Environmental Sciences, Thorvaldsensvej 40, 1871, Frederiksberg C, Denmark

[‖] Department of Physics, Chemistry and Pharmacy, University of Southern Denmark, Campusvej 55, 5230 Odense M, Denmark

[‡] Department of Chemistry, University of Copenhagen, 2100 Copenhagen, Denmark

[†] Université de Lorraine, CNRS, LCPME, 54600 Nancy, France

* Corresponding Author (Changyong Lu): clu@plen.ku.dk

Abstract

Layered double hydroxides (LDH) and their magnetic composites have been intensively investigated as recyclable high-capacity phosphorus (P) sorbents but with little attention to their stability as function of pH and phosphate concentration. The stability of a Fe_3O_4@SiO_2-Mg_3Fe LDH P sorbent as function of pH (5-11) and orthophosphate (P_i) concentration (1-300 mg P/L) was investigated. The composite has high adsorption capacity (approx. 80 mg P/g) at pH 5 but with fast dissolution of the LDH component resulting in formation of ferrihydrite evidenced by Mössbauer spectroscopy. At pH 7 more than 60 % of the LDH dissolves within 60 min, while at alkaline pH, the LDH is more stable but with less than 40 % adsorption capacity as compared to pH 5. The high P_i sorption at acid to neutral pH is attributed to P_i bonding to the residual ferrihydrite. Under alkaline conditions P_i is sorbed to LDH at low P_i concentration while magnesium phosphates form at higher P_i concentration evidenced by solid-state ^{31}P MAS NMR, powder X-ray diffraction and chemical analyses. Sorption as function of pH and P_i concentration has been fitted by a Rational 2D function allowing for estimation of P_i sorption and precipitation. In conclusion, the instability of the LDH component limits its application in wastewater treatment from acid to alkaline pH. Future use of magnetic LDH composites requires substantial stabilisation of the LDH component.

Key words: phosphate removal, pH effect, phosphate concentration, LDH dissolution, ferrihydrite, precipitation.

1. Introduction

Phosphorus in the form of orthophosphate is a limited resource which is mainly used as fertilizer and critical for feeding the world population [1, 19, 20]. Phosphorus use is highly unsustainable with substantial parts of phosphorus wasted and going out of circulation [2], and at the same time phosphorus overuse and poor control via waste streams have caused widespread eutrophication. The presence of trace amounts of phosphate in discharged wastewater may trigger eutrophication, leading to poor water quality, toxic algal blooms, and ecosystem destabilization [21]. Toxic algal blooms leads to accumulation of toxic cyanopeptides produced by cyanobacteria [22]. Thus, phosphorus emission reduction and management is one of the UN sustainability goals [3]. The EU Water Framework defines a cut-off total P concentration for lake eutrophication at 0.1 mg P/L, while WHO set this threshold concentration at 0.05 mg P/L (here the phosphate concentration is given in terms of mass of P (in phosphate) per liter [23, 24]. Thus, development of a phosphorus capture and recovery technology has high priority.

Phosphate removal from wastewater by adsorption is an alternative to chemical precipitation and biological treatment methods. Adsorption processes are often easier to control, faster, cheaper and scalable compared with often more complex precipitation and biological methods [25-30]. Layered double hydroxide (LDH) with the general formula of $[M_a^{II}{}_{1-x}M_b^{III}{}_x(OH)_2]^{x+}[A_{x/n}\cdot yH_2O]^{x-}$, where M_a^{II}, M_b^{III} and A^{n-} are di- and trivalent metal cations and n^- valent anion respectively [4], have been intensively investigated as P_i sorbents because of their anion exchange property, high sorption capacity and fast sorption kinetics [5-7]. In general, P_i sorption to LDH mainly takes part via electrostatic interactions, interlayer anion exchange, and surface complex formation [8-12]. P_i could also be removed

via precipitation, e.g. with use of CaFe and CaAl LDHs [9]. LDH and its composites have high P_i sorption capacity, ranging from 50 mg P/g to 100 mg P/g, at weak acid (pH 6) to intermediate pH (pH 7~8) [13]. On the contrary, they have low P_i sorption capacity at high pH (pH 9 ~ 10), typically lower than 5 mg P/g (Table S1). Moreover, the type of interlayer ion may affect the sorption capacity. For example carbonate and sulfate decrease the adsorption capacity compared with nitrate and chloride due to competitive ion-exchange [14]. The lamellar structure and the sub- to micrometer size of LDH particles make them difficult to be used in packed filter columns and even to collect by filtration or sedimentation [9]. However, by attaching the LDHs to magnetic nanoparticles such as magnetite, the magnetic composites can be separated in a magnetic field and thus be regenerated after P_i sorption [15]. Examples of such magnetic LDH P sorbents comprise magnetic nanoparticle decorated ZnFeZr LDH [15], MgAl LDH [16] and MgFeZr LDH [17] composites (Table S1).

LDHs are known to buffer pH due to dissolution in water with release of hydroxide (and metal) ions [18]:

$$[M^{II}_{a_{1-x}}M^{III}_{b_x}(OH)_2]^{x+}\left[A^{n-}_{\frac{x}{n}}\cdot yH_2O\right]^{x-}(s) \leftrightharpoons (1-x)M^{2+}_a(aq) + xM^{3+}_b(aq) + \frac{x}{n}A^{n-} + 2OH^- + yH_2O \quad \text{Equation 1}$$

Note, that the trivalent metal ions which are produced would form (hydr)oxide precipitates due to the negligible solubility of M_b^{III} hydroxides/oxides. The extent and rate of dissolution of the LDH is controlled by the nature of the divalent metal cations and the interlayer anions [31-33]. For example, the LDHs are strongly thermodynamically favored

over the separate M_a hydroxides in the order $Mg^{2+} < Mn^{2+} < Co^{2+} \approx Ni^{2+} < Zn^{2+}$, when Cl^- is the interlayer anion [32].

Environmentally benign materials are required for water cleaning. This limits the suitable LDH candidates for wastewater treatment to MgAl, MgFe, CaAl, CaFe and Fe(II)Fe(III) LDH [35]. Despite a vast number of publications on LDH P_i sorbents, the stability of LDHs for practical applications has not been evaluated. Most waste waters have pH in the range from 6.5 to 8.5 [34], which clearly would challenge the use of LDH as recyclable sorbents in magnetic composites due to the solubility of the LDH phase. For example, the well studied Fe_3O_4/MgAl-NO_3 LDH composite showed 33% dissolution of Mg over 6 h in a sorption study with initial pH at 7 In a study of synthetic MgAl and ZnAl LDHs for P recovery from urine, 12% of Mg and even more Zn dissolved during sorption at constant pH 8 for 24 h P_i sorption to hydrocalumite-type CaAl and CaFe LDH showed ready dissolution of LDH and formation of $Ca_5(PO_4)_3OH$ and $Ca(HPO_4)\cdot 2H_2O$ precipitates in non-buffered solutions [12, 36]. MgFe-CO_3 LDH dissolved completely with formation of $MgHPO_4\cdot 3H_2O$ in 24h when exposed to very high P_i concentrations (> 1 M) at pH 7, demonstrating that not only the pH but also the high P_i concentration could also stimulate the dissolution of LDH. For P_i sorption at pH where the LDH dissolves, residual M_b (hydr)oxides may form strong sorbents of P_i. Thus, P_i retention by LDHs not only comprise anion exchange and surface complexation by the LDH, but may also comprise P_i sorption to dissolution residues and precipitation processes, see Fig. 1.

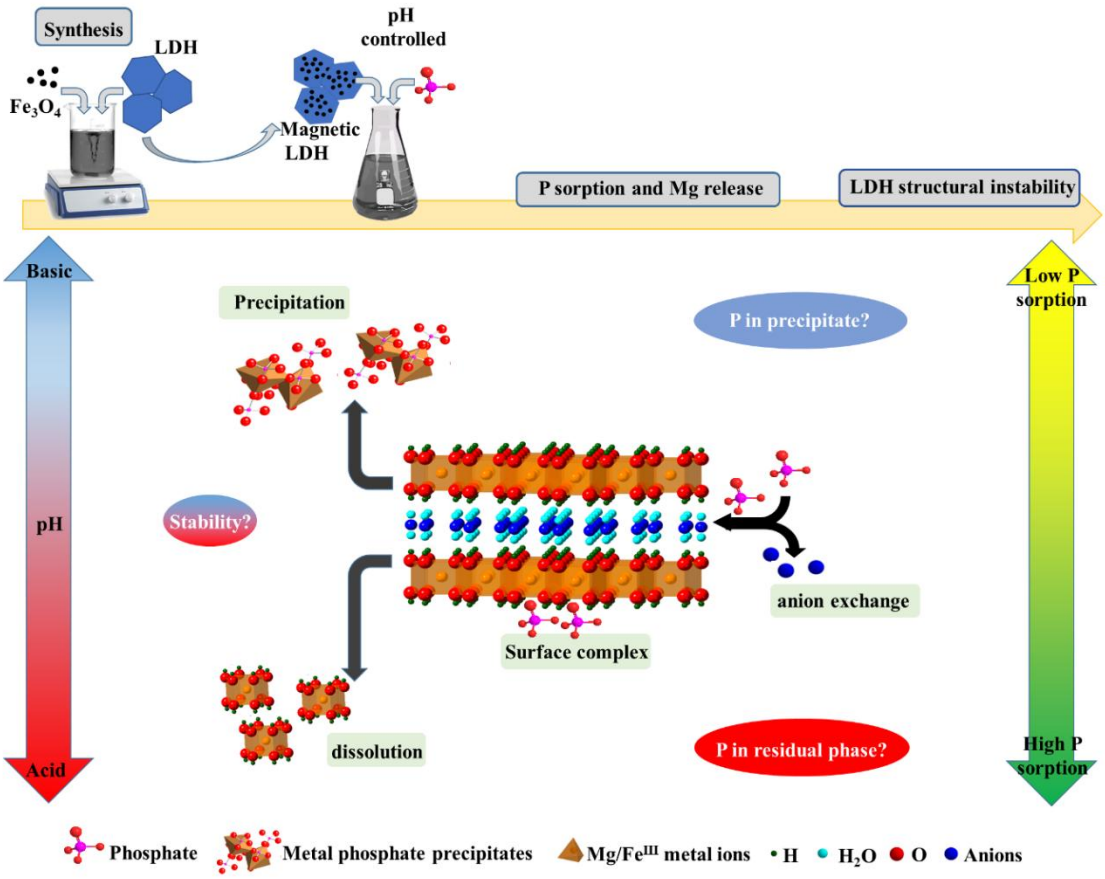

Figure 1. Schematic illustration of the phase changes and P_i sorption processes addressed in the study.

The instability of the LDH may hamper regeneration and re-use of the LDH during P_i sorption, but to which extent is still unclear. Although P_i sorption to MgFe-LDH has been extensively studied due to its high sorption capacity compared with MgAl LDH [17, 37], its stability and mode of P_i sorption at pH and P_i concentrations in wastewater needs to be critically examined. In this study, we aim to assess the stability of the potential recyclable magnetic MgFe LDH sorbent as a function of pH and P_i concentration (Fig. 1). The investigation focus on quantification of LDH dissolution as a function of pH (especially at pH neutral) and P_i sorption combined with solid-state analysis of alteration in the MgFe LDH structure and formation of new phases during sorption.

2. Materials and methods

2.1 Materials

All chemicals were purchased from Sigma and directly used without further purification. All sample solutions were prepared with ultrapure water (18.2 MΩ·cm) (SI 1.1).

2.2 Synthesis of Fe_3O_4@SiO_2-Mg_3Fe LDH

The Fe_3O_4@SiO_2-Mg_3Fe LDH composite (referred to as composite in this paper) was synthesized by previous reported methods [35, 37, 38]. For experimental details, see SI (1.2).

2.3 Phosphate sorption and Fe_3O_4@SiO_2-Mg_3Fe LDH dissolution

Experiment 1 (Exp. 1) The kinetics of P_i sorption and LDH dissolution from the composite was followed by monitoring the P_i and Mg concentrations in pH buffered suspensions. The composite (1 g/L) was dispersed in an aqueous solution of 10 mM KNO_3 electrolyte, 11.92 g/L HEPES buffer and 50 mg P/L added as KH_2PO_4. The pH of the solution was buffered by HEPES at pH 7.2 throughout the experiment. At various times (1, 2, 5, 10, 30 min, 1, 2, 3, 6, 12 and 24 h), 2 mL of the suspension was sampled and filtered through a 0.2 μm regenerated cellulose filter (Mikrolab Aarhus A/S) and the filtrate stored at 4 ℃ until determination of P_i and Mg. In a separate experiment, the pH buffering effect of the composite was illustrated by preparing the same suspension as above but without adding HEPES buffer. The pH of the suspension was measured at 1, 2, 5, 10, 30 min, 1, 2, 3, 6, 12 and 24 h.

Experiment 2 (Exp. 2) In this experimental series dissolution and P_i sorption of the composite as function of solution P_i concentration and pH was studied. The experiments were carried out as described for Exp. 1, but with initial P_i concentrations at 1, 2, 5, 10, 20, 50, 100, 200 and 300 mg P/L. No HEPES buffer was used, but suspension pH was controlled at 5, 7, 9 and 11 by addition of HCl or NaOH solution (SI 1.3). All suspensions were placed on a shaking table at 250 rpm for 24 h once the pH had stabilized.

Experiment 3 (Exp. 3) This experiment was similar to Exp. 2 but only P_i concentrations of 10 mg P/L was tested to avoid side reactions due to high P_i concentrations and to operate with P_i concentrations typical for wastewater influents [3]. In addition equilibration time was reduced to 1 h to have short contact time for real waste water treatment [39]. The pH of the suspensions was controlled at pH 5, 6, 7, 8, 9, 10 or 11 (± 0.1) by addition of HCl or NaOH solution (SI 1.3).

The solid phases were collected by an NdFeB magnet after P_i sorption and dried at 60℃ overnight, while the solutions were filtered through 0.2 μm regenerated cellulose filter (Mikrolab Aarhus A/S) and stored at 4 ℃. P_i and Mg concentrations were determined in all the filtrates. P_i concentrations in solution were measured by the Molybdenum-Blue method using a ultraviolet–visible spectroscopy (UV-Vis) and Mg was determined by Atomic Absorption Spectroscopy (AAS). The content of Mg in the solids after sorption was determined with ICP. For further information about solid state characterization techniques, see SI 1.5.

2.4 Solubility calculations

Visual MINTEQ equilibrium speciation software ver 3.1 was used to estimate supersaturation of solutions with respect to magnesium phosphates, such as $Mg_3(PO_4)_2$, $MgHPO_4$, $Mg(H_2PO_4)_2$. The thermodynamic database supplied with the software was used (SI 1.6).

2.5 P_i sorption and phase distribution versus pH and P_i concentration.

All sorption data from Exp. 2 were fitted to produce a "sorption surface" with sorbed P_i versus pH and equilibrium P_i concentration using the nonlinear surface fit function in Origin 9.6 software using a Rational 2D Function [40]. Fitting parameters are listed in Table S8.

The extent of P_i sorption in form of magnesium phosphate precipitates was estimated based on estimations of mass of LDH derived from PXRD traces of samples taken after P_i sorption. First, Rietveld profile-fitting in X'pert Highscore Plus software [41] with the Pseudo Voigt profile function was used to analyse the PXRD data (SI 1.5.3) to determine the amount of LDH and Fe_3O_4 in crystalline phases after P_i sorption (Exp. 2). Next, the theoretical concentration of Mg released was calculated (SI 5, Eq. S10), assuming that the Mg release is proportional to the amount of dissolved LDH. Last, the theoretical Mg release was compared with the observed Mg concentration after P_i sorption, and the difference between these two values was then allocated to Mg in magnesium phosphate precipitates (Details in SI5). Estimates of the fraction of P_i in magnesium precipitates (Eq. S11) was added to the "sorption surface" using OriginPro 2019 software.

3. Results and discussion

In this study, the Fe_3O_4@SiO_2-Mg_3Fe LDH composite was first synthesized and characterized in detail (SI 2), followed by P_i sorption and dissolution experiments at controlled pH, ranging from 5 to 11, with exposure to various solution P_i concentrations (1~300 mg P/L). Different solid state characterization techniques, such as PXRD, TEM, ^{57}Fe Mössbauer spectroscopy and ^{1}P MAS NMR were used to characterize the composite before and after P_i sorption. LDH dissolution in terms of Mg release and P_i sorption was correlated with solid phase analysis to conclude on dissolution, P_i phase distribution and modes of P_i sorption versus pH and P_i concentration.

3.1 Phosphate sorption to Fe_3O_4@SiO_2-Mg_3Fe LDH

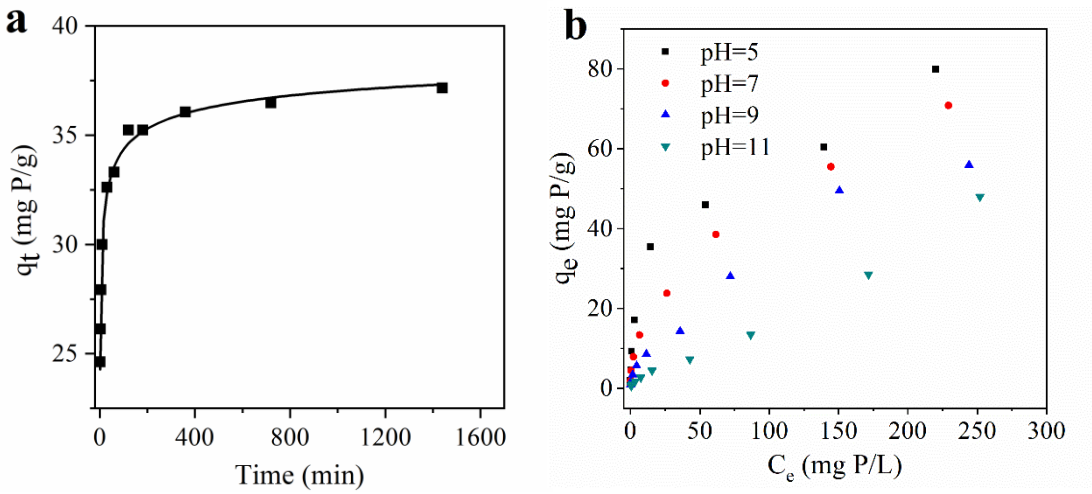

Figure 2. (a) Kinetics of P_i sorption (q_t) to Fe_3O_4@SiO_2-Mg_3Fe LDH and the corresponding fit by pseudo second-order kinetics (Eq. S4) (sorbent concentration 1 g/L; 50 mg P/L; pH 7.2, 25 ^{o}C). (b) Isotherms for P_i sorption (q_e) versus solution P_i concentration (C_e) at different pH values (sorbent concentration 1 g/L, contact time 24 h, Exp. 2).

After mixing with the pH buffered P_i solution (Exp. 1), the composite showed fast P_i sorption, which was well fitted by pseudo second-order kinetics (Eq. S4, R^2 0.999) with a rate constant of 5.4×10^{-3} g/mg P min^{-1}. Equilibrium was reached within 120 min (Fig. 2a), demonstrating relatively fast P_i removal. Sorption isotherms (Exp. 2) showed that P_i bonding to the composite was of the Freundlich type (Eq. S5, R^2 0.979~0.999 Table S2) with no clear sorption maxima (Fig. 2b). The P_i sorption capacity decreased remarkably with increasing pH from 5 to 11, with 3 to 8 times less sorption at pH 11 than pH 5 depending on the solution P_i concentration (Fig. 2b and 3b) which is similar with other observations in previous studies on LDHs P_i sorbents [42-44].

3.2 Dissolution of Fe_3O_4@SiO_2-MgFe LDH during P_i sorption

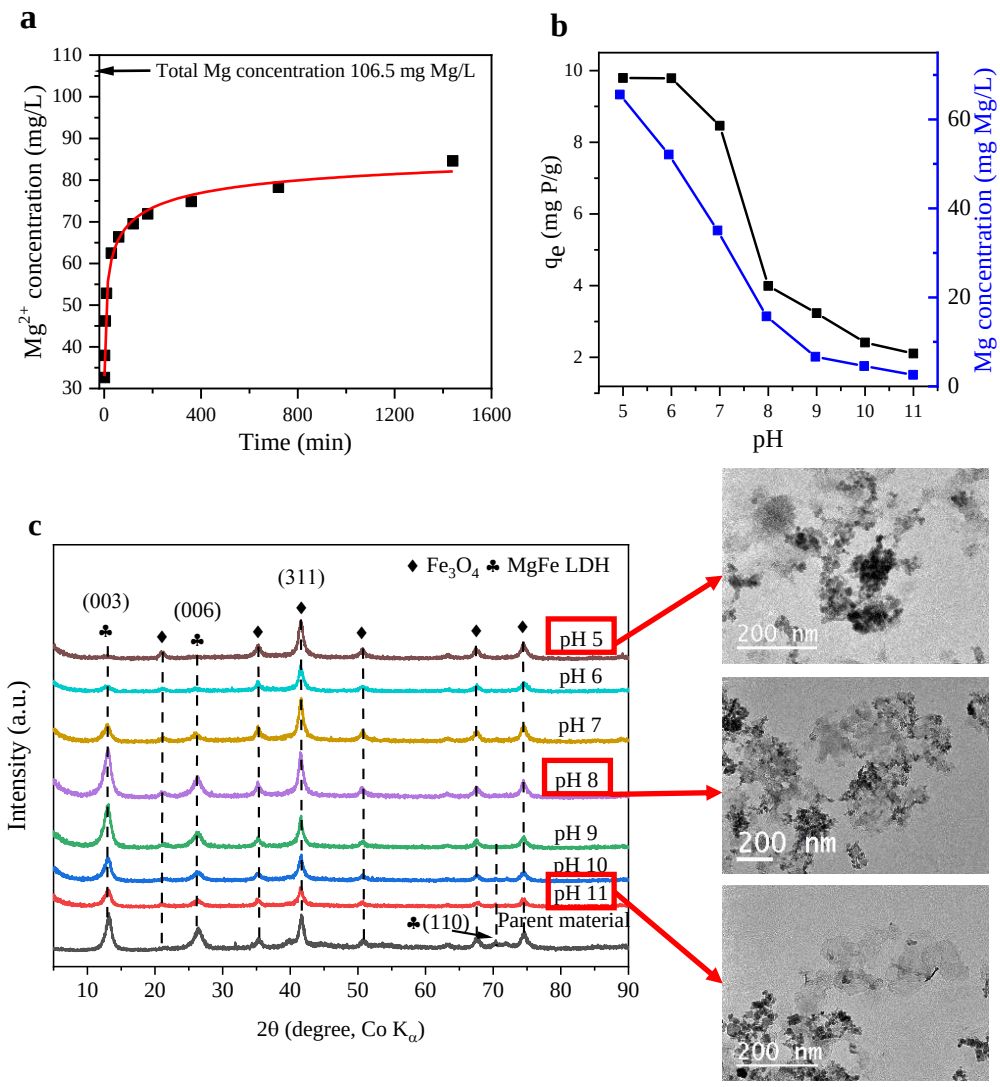

203

204 **Figure 3. (a) Kinetics of Fe_3O_4@SiO_2-Mg_3Fe LDH dissolution measured as the**
205 **concentration of Mg in the solution during P_i sorption (Exp. 1). (b) P_i adsorbed and**
206 **Mg released from the Fe_3O_4@SiO_2-Mg_3Fe LDH at different pH values (Exp. 3). (c)**
207 **PXRD patterns of the solids after sorption at different pH and the corresponding**
208 **TEM images of the solids after Exp. 3 at pH 5, 8 and 11.**

209 In Exp. 1, when the composite was dispersed in water, pH increased from 7.0 to 9.3 within
210 3 h (Fig. S6). This is attributed to release of hydroxide ions during dissolution of the LDH

211 (Eq. 1) [31, 45-47]. However, when pH is kept constant at pH 7.2 in HEPES buffered
212 solution, substantial parts of the Mg_3Fe LDH in the composite dissolves as more than 60 %
213 of the total Mg dissolves within 60 min (Fig. 3a). The kinetics of Mg release was well fitted
214 by pseudo second-order kinetic resulting in a kinetic constant of 2.6×10^{-3} L/mg min^{-1} (Eq.
215 S6; R^2 0.999), demonstrating fast dissolution at pH 7.2. This is in line with our previous
216 study of Zn doped MgFe LDH, which showed a similar fast dissolution kinetics (k =
217 2.53×10^{-3} L/mg min^{-1}) at pH 7 [46]. The PXRD data show a dramatic decrease in intensity
218 of the Mg_3Fe LDH reflections, compared with the LDH kept at pH 9.3 (Fig. S8). In
219 conclusion, both the solubility and the structural degradation of the LDH confirms that the
220 composite is unstable at pH 7.2 and dissolves rapidly.

221 In Exp. 3, the Mg_3Fe LDH stability was investigated in non-buffered solutions as function
222 of constant pH ranging between 5 and 11 at a constant initial P_i concentration of 10 mg P/L.
223 Fig 3b shows a dramatic decrease of P_i sorption with increasing pH. At pH 5, almost 100 %
224 of the P_i added is removed, while at pH 11 sorption is down to 20 %. In addition, the P_i
225 sorption is followed by a concurrent release of Mg depending on pH. More than 50 % of
226 total Mg was released at pH 5 but less than 3 % Mg released at pH 11 within 1 h. PXRD of
227 the composite after P_i sorption at pH > 8 (Fig. 3c) showed that the LDH basal (003)
228 reflection has a relative intensity of 96 % compared with the pristine composite (Fig. S2a),
229 demonstrating that the composite is stable at pH > 8 at low P_i concentration (10 mg P/L), in
230 agreement with our recent study [35]. However, at lower pH of 7, 6 and 5 the relative
231 intensity of the basal reflections dropped to 37%, 20% and 0 % of the initial values,
232 respectively (Fig. 3c). TEM images of the sorbents after P_i sorption (Fig. 3c) reveal a full
233 destruction of the LDH and formation of amorphous material at pH 5, while at pH 8 more

LDH remained, but still with some amorphous material present compared with the pristine LDH (Fig. S2). At pH 11, the intact Mg_3Fe LDH is present. In addition, the LDH platelet thickness estimated from the width of the (003) reflections was in the range 6.9-7.1 nm for pH > 8, and decreased to 5.3 nm, 4.6 nm and 0 nm when P_i had sorbed at pH 7, 6 and 5, respectively (Table S3), due to dissolution. Thus, Mg_3Fe LDH dissolves at acidic to intermediate pH, while it is stable at high pH.

The combined effect of pH and P_i sorption on LDH dissolution is depicted in Fig. S10, showing that about 90, 80 and 40 % of total Mg has dissolved at the highest P_i sorption at pH 5, 7 and 9, respectively. PXRD of the residual solids after P_i sorption (Fig. S11 and Fig. S12) showed a dramatic decrease in intensity of the LDH reflections in the samples from pH 5 and 7 (Fig. S11a, b; Fig. S2a), confirming the instability of the LDH structure at acid and neutral pH [35, 46]. Furthermore, the (003) and (110) reflections of the Mg_3Fe LDH phases weakened or disappeared when initial P_i concentrations exceeded 50 mg/L at higher pH, such as pH 9 and 11, revealing that exposure to relative high P_i concentrations also stimulated LDH dissolution (Fig. S11c, d and Fig. S12) [35, 48]. Finally, magnetization data shows that the fraction of magnetic materials decreases from 66 to 45 wt% in the composite after P_i sorption at pH 5 (Fig. S13a and b, Eq. S9).

3.3 Residual phase formed at pH 5

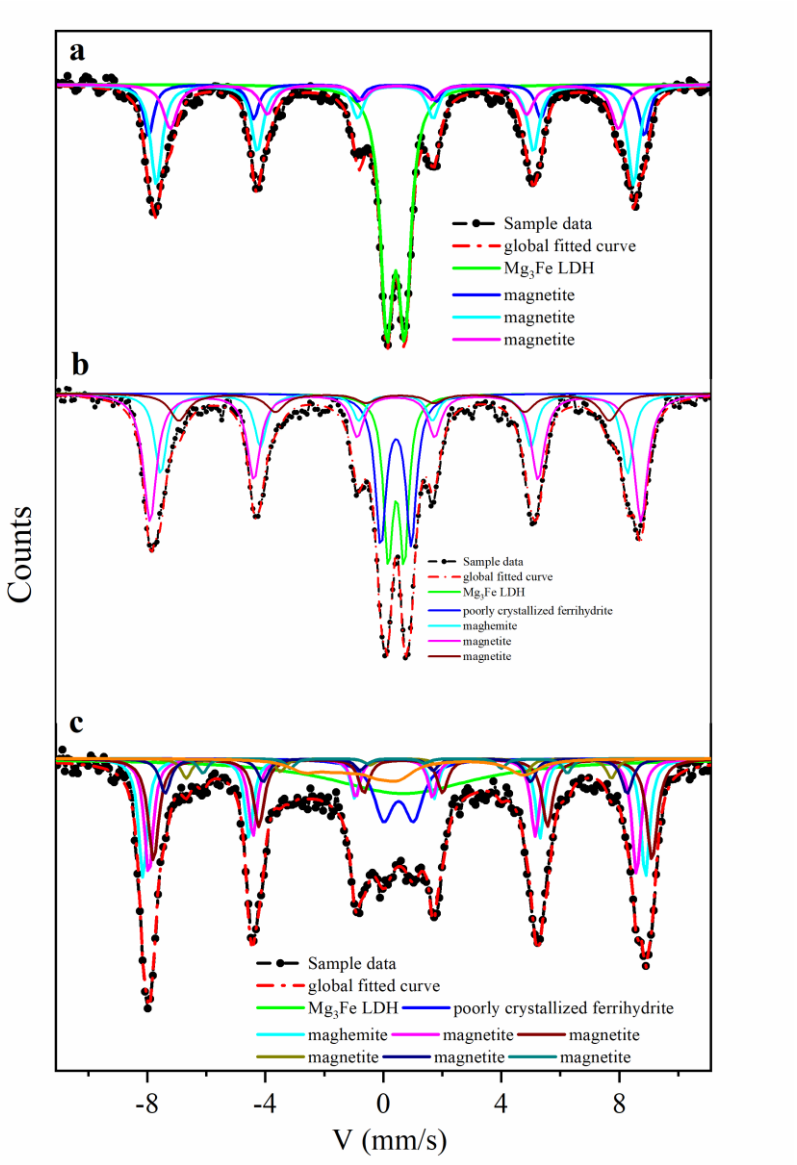

Figure 4. Mössbauer spectra of Fe_3O_4@SiO_2-Mg_3Fe LDH before P_i sorption measured at 140K (a), after P_i sorption (Exp. 3) (at pH 5 with initial P_i concentration at 10 mg P/L for 1h) measured at 125K (b) and 25K (c) (Full lines correspond to fitting, parameters listed in Table S4).

The ^{57}Fe Mössbauer spectrum of the pristine composite at 140 K (Fig. 4a) shows one sharp quadrupole doublet with center shift (δ) 0.42 mm/s and quadrupole splitting (Δ) of 0.61 mm/s which is attributed to octahedrally coordinated Fe^{3+} in the Mg_3Fe LDH [49]. The 125

K spectrum of the composite after P_i sorption (Fig. 4b) displays two quadrupole doublets with the same δ of 0.45 mm/s and different Δ of 0.54 mm/s and 1.03 mm/s, respectively. The Δ of 0.54 mm/s corresponds to the presence of Mg_3Fe LDH, while the Δ of 1.03 mm/s corresponds to presence of Fe^{3+} in poorly crystalized ferrihydrite [50]. The 25 K spectrum (Fig. 4c) confirms this identification with a contribution of a single-line with δ of 0.68 mm/s and a magnetic broad sextet with Δ of 2 mm/s and very low magnetic field of 132 kOe attributed to poorly crystalized ferrihydrite [50].

The high sorption capacity at low pH (79.5 mg P/g in Fig. 1b) is in agreement with the high sorption capacity for ferrihydrite at low pH [51-54]. Thus, we estimate the obtained poorly crystalized ferrihydrite has a P_i sorption capacity around 344 mg P/g (details in SI 3), which is much higher than common values (34~56 mg P/L) reported for ferrihydrite [54, 55]. We attribute this high sorption capacity to the possible formation of amorphous strengite ($FePO_4$) [56, 57] as the Fe:P ratio is close to 1:1. Apparently, extensive Mg dissolution causes formation of ultra-small ferrihydrite particles, leading to a strengite type product [58].

3.4 Precipitation of magnesium phosphates at high pH

In Exp. 2, although the composite did not release more than about 40% of total Mg into solution at pH 9 at an initial P_i concentration of 300 mg P/L (Fig S10), the LDH structure was almost destroyed as seen from the PXRD pattern (Fig. S11c). At pH 11, there was barely any Mg release to solution (Fig. S9), while the relative intensity of the Mg_3Fe LDH (003) and (110) peaks decreased to 26 % and 59 % of the intensity of the pristine composite, respectively (Fig. S11d, Fig. S12), reflecting substantial disslution of the LDH phase.

282 According to the previous studies of MgFe-CO_3 LDH [48], precipitation of magnesium
283 phosphates is therefore likely to take place. In order to test this, the solids after P_i sorption
284 at pH 11 and initial P_i concentration of 300 mg P/L were examined by PXRD without prior
285 washing (Fig. S14). This test confirmed the partial dissolution of the Mg_3Fe LDH phase
286 seen from the decrease in intensity of basal reflections. Also, the size of crystallite domains
287 of the Mg_3Fe LDH phase along the ab-plane and c-axis was 33 % and 66 % smaller after P_i
288 sorption than before as determined from peak broadening (Eq. S3; SI 2). Solid-state ^{31}P
289 MAS NMR spectroscopy (Fig. S15) of the LDH after P_i sorption at pH 9 and 11 showed
290 the presence of narrow resonance with $\delta(^{31}P)$ = 2.5(2) ppm and 3.9(2) ppm at pH 9 and pH
291 11, respectively, demonstrating formation of an amorphous magnesium phosphate phase
292 [35]. The Mg-P precipitate had a molar Mg/P ratio in the Mg-P precipitates of 1.4 (SI 5),
293 which is in good agreement with formation of $Mg_3(PO_4)_2$. Thus, at high pH and elevated P_i
294 concentrations LDH dissolves and magnesium phosphates precipitate.

295 Visual MINTEQ was used to compute supersaturation with respect to magnesium
296 phosphates using the measured solution Mg and P_i concentrations at different pH (Fig. S17).
297 No magnesium phosphates form at pH < 6, but when pH is increased to 7, $MgHPO_4 \cdot 3H_2O$
298 precipitate at high Mg and P_i concentrations, while $Mg_3(PO_4)_2$ precipitate at pH > 8 at high
299 P_i concentration. When pH is further increased to 9, $Mg_3(PO_4)_2$ precipitate at P_i
300 concentrations above 62.5 mg P/L, which is in line with the observations in Fig. S10 and
301 S11c. When pH increased to 11, $Mg_3(PO_4)_2$ precipitate even at low P_i concentrations (1 mg
302 P/L). Thus, VMINTEQ calculations confirm that magnesium phosphates precipitate at high
303 pH and high P_i concentrations with $Mg_3(PO_4)_2 \cdot 8H_2O$ as a likely phase. Hence, at

intermediate to high pH, P_i may also be retained due to the dissolution-precipitation reaction [32].

$$Fe(\mathrm{III})_x Mg_{1-x}(OH)_2(NO_3)_x \leftrightharpoons xFe(\mathrm{III})(OH)_3 + (1-x)Mg^{2+} + 2 \times OH^- + xNO_3^- \quad (1)$$

$$3Mg^{2+} + 2PO_4^{3-} + xH_2O \rightarrow Mg_3(PO_4)_2 \cdot xH_2O \downarrow \quad (2)$$

3.5 P_i sorbed to Fe_3O_4@SiO_2-Mg_3Fe LDH versus pH and equilibrium P_i concentration

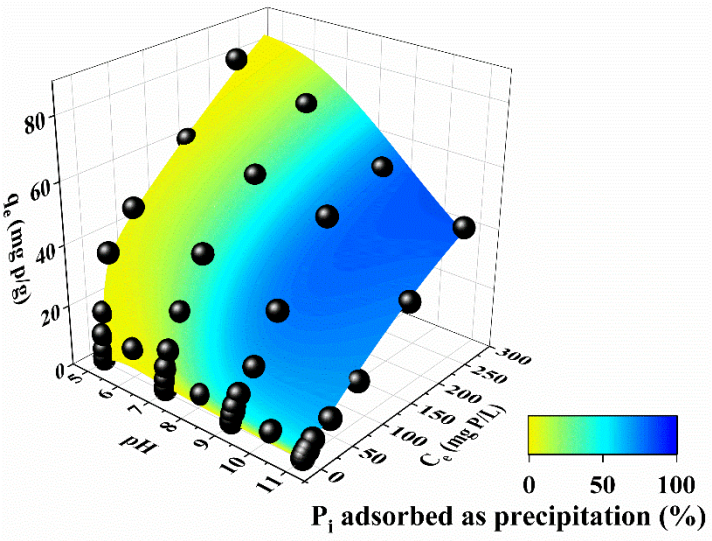

Figure 5. Sorbed P_i (black dots) to Fe_3O_4@SiO_2-Mg_3Fe LDH as a function of pH and P_i solution concentration (Exp. 2 and 3; SI 5) with Rational 2D fit. The colour bar denotes the estimated percentage (%) of P_i sorbed due to precipitation.

Our investigation shows that P_i sorption by Fe_3O_4@SiO_2-Mg_3Fe LDH comprises at least three reactions: P_i bonding to iron hydroxides (ferrihydrite), bonding to LDH and precipitation of magnesium phosphates. By fitting the P_i sorption data with the Rational 2D function ($R^2 = 0.99$), a sorption surface (Fig. 5) can be produced to help estimate P_i sorption

versus pH and equilibrium P_i concertation. The colour map shows that barely no P_i was removed by precipitation at acid and neutral pH (Fig. 5). When pH increased to 9, at least 40 % of sorbed P_i was present in magnesium phosphates at P_i concentrations > 50 mg P/L, further increasing at higher pH and P_i concentrations.

We propose a set of sorption pathways for P_i bonding to the composite (Fig. 6). At acidic pH, the LDH is readily and fully dissolved. Despite high Mg concentrations in solution, the solubility of magnesium phosphates does not exceeded saturation and hence P_i is adsorbed to the amorphous poorly crystalized ferrihydrite. At neutral pH, the LDH only partially dissolves. Hence, P_i is sorbed on the remaining LDH as well as to the poorly crystalized ferrihydrite; at higher P_i concentrations, P_i is also retained due to precipitation of magnesium phosphates. Finally, at alkaline pH where the LDH phase has its highest stability, Mg_3Fe LDH is the primary sorbent of P_i at low P_i concentration. However, at higher P_i concentration, the Mg_3Fe LDH phase is not stable and magnesium phosphates precipitate is the main sorption pathway.

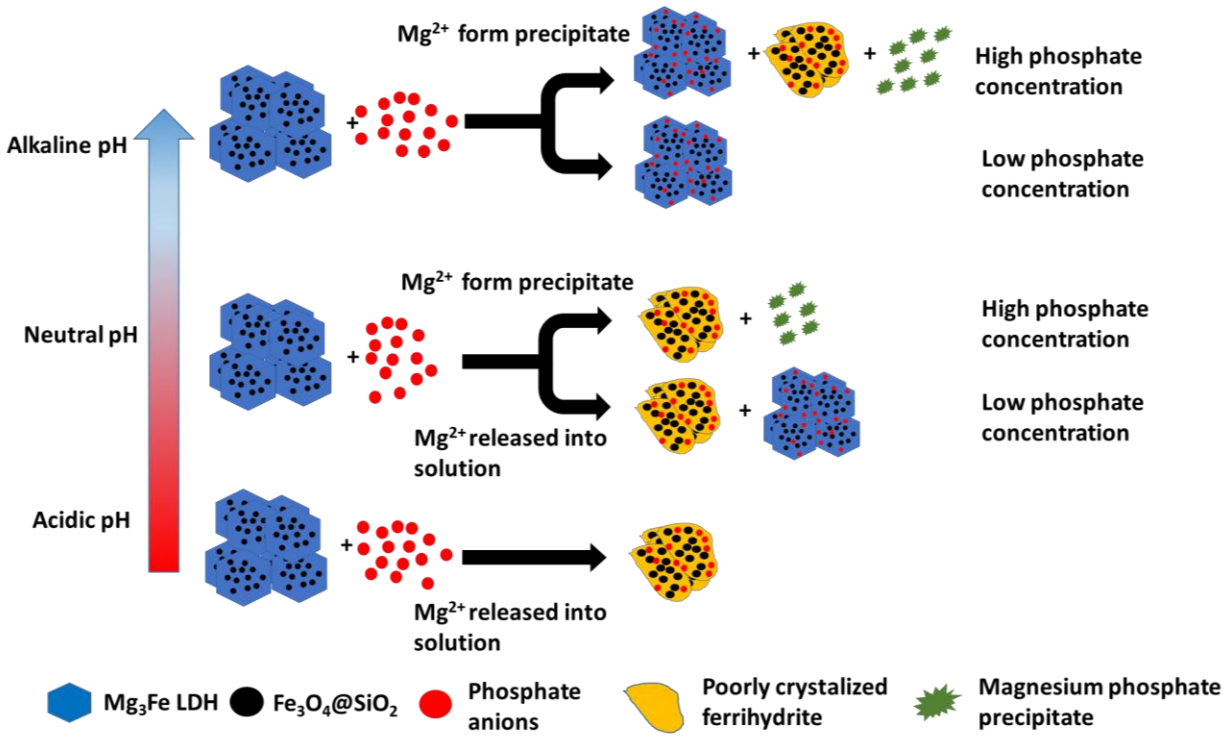

Figure 6. Pathways for P_i sorption to Fe_3O_4@SiO_2-Mg_3Fe LDH at various pH and P_i concentrations.

The instability of MgFe LDH we have seen is comparable to what have been observed in other studies even without constant pH control and the pH was buffered to alkaline condition. A MgAl LDH was found to release 20 % of Mg within 72 h even at pH 9.[12] Recent study of P_i sorption to MgFe-NO_3 LDH showed precipitation of amorphous magnesium phosphate precipitate at a solution P_i of about 100 mg P/L at pH 7.4 [35]. The solubility of LDHs decrease with the divalent cation in the order $Mg^{2+} > Mn^{2+} > Co^{2+} \approx Ni^{2+} > Zn^{2+}$, while for the trivalent cation the order is $Fe^{3+} > Al^{3+}$ [32]. Hence, many Fe^{3+} containing LDHs have higher or equal solubility as the MgFe-LDH. Most stable LDHs would be of the type with Co^{2+} or Ni^{2+} as divalent cation [59]. However, these compounds are not environmentally friendly. Solubility and dissolution kinetics may be decreased using larger particles and using carbonate interlayered forms rather than forms with

monovalent anions [60-62]. On the other hand, the presence of complexing agents in solution such as humic matter will increase solubility [63].

Although LDHs are seen as promising material for treatment of municipal wastewater [64], the significant dissolution of LDHs filter material during the sorption process at neutral pH limits its practical application as wastewater has pH 6.5~8.5 [34]. Vast amounts of Mg^{2+} ions could be released to the environment in a scaled-up application, which would increase water hardness and block the filters and pipes due to formation of precipitates. In addition, the loss of relative expensive MgFe LDH materials would also increase the cost of wastewater treatment. Furthermore, high P_i concentrations in wastewater would also stimulate the dissolution of LDHs at higher pH resulting in formation of precipitates. Thus, the widely reported LDH regeneration and P recovery strategy, where adsorbed P is extracted with alkali solution and the LDH re-used for P sorption, would be challenged [15, 65].

4. Conclusions

In this study, we demonstrate the MgFe LDH has poor stability and dissolves in the pH range of wastewater (pH 6~8). In addition to the pH controlled LDH solubility, high P_i concentrations causes LDH dissolution even at high pH, by formation of magnesium precipitates. ^{57}Fe Mössbauer spectroscopy confirms the formation of poorly crystalized ferrihydrite at acid pH while ^{31}P MAS NMR spectroscopy demonstrate the precipitation of magnesium phosphate at high pH and high P_i concentration. A combined analysis of solubility and PXRD data indicate that precipitates is the main sorption pathway at high pH and high P_i concentration. The main sorption pathways are summarized as sorption by

ferrihydrite at acid pH, sorption by ferrihydrite and LDH at neutral pH and high pH with low P_i concentration, and precipitation of magnesium phosphates at high pH and high P_i concentration. This study demonstrates that LDHs are intrinsically unstable from pH 5 ~ 11 when used for P_i sorption which hence prevents there use as recyclable sorbents. Future application of magnetic LDHs as recyclable sorbents is only possible if the stability of the LDH component can be substantially increased.

Acknowledgement

We acknowledge the Danish Research Council for the financial support of this project (MagS^3, Project Number 1129331001) and the Villum Foundation for the ^{31}P NMR analysis in the Villum center for bioanalytical sciences (600 MHz NMR spectrometer). We greatly thank our laboratory technicians Birgitte Boje Rasmussen and Anita Schjødt Sandager for assistance with ICP and AAS.

Appendix supplementary data

The supplementary data of this paper is available on the website at DOI:

REFERENCES

[1] K.A. Wyant, J.E. Corman, J.J. Elser, Phosphorus, food, and our future, Oxford University Press, 2013.
[2] R.W. Scholz, A.E. Ulrich, M. Eilittä, A. Roy, Science of The Total Environment 461-462 (2013) 799-803.
[3] Science for Environment Policy Indepth Report: Sustainable Phosphorus Use. Report produced for the European Commission DG Environment, Science Communication Unit, University of the West of England, 2013.
[4] G. Mishra, B. Dash, S. Pandey, Applied Clay Science 153 (2018) 172-186.
[5] Q. Wang, D. O'Hare, Chemical Reviews 112 (2012) 4124-4155.
[6] E.M. Seftel, R.G. Ciocarlan, B. Michielsen, V. Meynen, S. Mullens, P. Cool, Applied Clay Science 165 (2018) 234-246.

[7] J.-H. Kim, J.-K. Kang, S.-C. Lee, S.-B. Kim, Applied Clay Science 170 (2019) 1-12.
[8] Y. Xu, Y. Dai, J. Zhou, Z.P. Xu, G. Qian, G.Q.M. Lu, Journal of Materials Chemistry 20 (2010) 4684-4691.
[9] K.-H. Goh, T.-T. Lim, Z. Dong, Water Research 42 (2008) 1343-1368.
[10] G. Darmograi, B. Prelot, A. Geneste, G. Martin-Gassin, F. Salles, J. Zajac, The Journal of Physical Chemistry C 120 (2016) 10410-10418.
[11] L. Lundehøj, J. Cellier, C. Forano, U.G. Nielsen, The Journal of Physical Chemistry C 123 (2019) 24039-24050.
[12] M. Al Jaberi, M. Mallet, H.C. Greenwell, M. Abdelmoula, C. Ruby, Applied Clay Science 182 (2019) 105281.
[13] S. Cheng, L. Shao, J. Ma, X. Xia, Y. Liu, Z. Yang, C. Yang, S. Li, Environmental Science: Nano 6 (2019) 2615-2625.
[14] H. Hatami, A. Fotovat, A. Halajnia, Applied Clay Science 152 (2018) 333-341.
[15] A. Drenkova-Tuhtan, M. Schneider, M. Franzreb, C. Meyer, C. Gellermann, G. Sextl, K. Mandel, H. Steinmetz, Water Research 109 (2017) 77-87.
[16] C.-G. Lee, S.-B. Kim, Environmental Technology 34 (2013) 2749-2756.
[17] A. Drenkova-Tuhtan, K. Mandel, A. Paulus, C. Meyer, F. Hutter, C. Gellermann, G. Sextl, M. Franzreb, H. Steinmetz, Water Research 47 (2013) 5670-5677.
[18] Y.-F. Lung, Y.-S. Sun, C.-K. Lin, J.-Y. Uan, H.-H. Huang, Scientific Reports 6 (2016) 32458.
[19] E. Valsami-Jones, Phosphorus in Environmental Technology: Principles and Applications, IWA Publishing, 2005.
[20] R. Lal, B.A. Stewart, Soil phosphorus, CRC Press, 2016.
[21] K. Ashley, D. Cordell, D. Mavinic, Chemosphere 84 (2011) 737-746.
[22] E.M.L. Janssen, Water Research 151 (2019) 488-499.
[23] G. Lyngsie, K. Katika, I.L. Fabricius, H.C.B. Hansen, O.K. Borggaard, Chemosphere 222 (2019) 884-890.
[24] J. Bartram, I. Chorus, Toxic cyanobacteria in water: a guide to their public health consequences, monitoring and management, CRC Press, 1999.
[25] A. Othman, E. Dumitrescu, D. Andreescu, S. Andreescu, ACS Sustain. Chem. Eng. 6 (2018) 12542-12561.
[26] Q.S. Si, Q. Zhu, Z.P. Xing, ACS Sustain. Chem. Eng. 5 (2017) 11422-11432.
[27] H.-S. Park, S.-H. Kwak, D. Mahardika, N. Mameda, K.-H. Choo, Chemical Engineering Journal 319 (2017) 240-247.
[28] P.S. Kumar, L. Korving, M.C.M. van Loosdrecht, G.-J. Witkamp, Water Research X 4 (2019) 100029.
[29] B. Wu, J. Wan, Y. Zhang, B. Pan, I.M.C. Lo, Environmental Science & Technology 54 (2020) 50-66.
[30] H. Ohtake, S. Tsuneda, Phosphorus recovery and recycling, Springer, 2019.
[31] M. Jobbágy, A.E. Regazzoni, Applied Clay Science 51 (2011) 366-369.
[32] J.W. Boclair, P.S. Braterman, Chemistry of Materials 11 (1999) 298-302.
[33] L. Bhattacharya, E. Elzinga, Soil Systems 2 (2018) 20.
[34] M. Pescod, (1992).
[35] T.-H. Kim, L. Lundehøj, U.G. Nielsen, Applied Clay Science 189 (2020) 105521.
[36] B. Bekele, L. Lundehøj, N.D. Jensen, U.G. Nielsen, C. Forano, Applied Clay Science 176 (2019) 49-57.
[37] K. Mandel, A. Drenkova-Tuhtan, F. Hutter, C. Gellermann, H. Steinmetz, G. Sextl, Journal of Materials Chemistry A 1 (2013) 1840-1848.
[38] F. Cavani, F. Trifirò, A. Vaccari, Catalysis Today 11 (1991) 173-301.

[39] Q. Xie, Y. Li, Z. Lv, H. Zhou, X. Yang, J. Chen, H. Guo, Scientific Reports 7 (2017) 3316.
[40] J.M. Daul, V.A. Kazakov, I.K. Kostov, Nuclear Physics B 409 (1993) 311-338.
[41] B. PANalytical, X'Pert HighScore Plus, Lelyweg, Almelo, the Netherlands 2 (2002).
[42] R. Chitrakar, S. Tezuka, J. Hosokawa, Y. Makita, A. Sonoda, K. Ooi, T. Hirotsu, Journal of Colloid and Interface Science 349 (2010) 314-320.
[43] Y. Guo, Z. Zhu, Y. Qiu, J. Zhao, Journal of Environmental Sciences 25 (2013) 944-953.
[44] S. Wan, S. Wang, Y. Li, B. Gao, Journal of Industrial and Engineering Chemistry 47 (2017) 246-253.
[45] J. Shibata, N. Murayama, S. Nakajima, KAGAKU KOGAKU RONBUNSHU 33 (2007) 273-277.
[46] A. Imran, S. López-Rayo, J. Magid, H.C.B. Hansen, Applied Clay Science 123 (2016) 56-63.
[47] Y. Seida, Y. Nakano, Water Research 36 (2002) 1306-1312.
[48] Y. Du, N. Rees, D. O'Hare, Dalton Transactions (2009) 8197-8202.
[49] P. Refait, M. Abdelmoula, F. Trolard, J.-M.R. Génin, J.J. Ehrhardt, G. Bourrié, American Mineralogist 86 (2001) 731-739.
[50] J. Filip, R. Zboril, O. Schneeweiss, J. Zeman, M. Cernik, P. Kvapil, M. Otyepka, Environmental Science & Technology 41 (2007) 4367-4374.
[51] R. Chitrakar, S. Tezuka, A. Sonoda, K. Sakane, K. Ooi, T. Hirotsu, Journal of Colloid and Interface Science 298 (2006) 602-608.
[52] A. Chen, Y. Arai, Environmental Science & Technology 53 (2019) 8205-8215.
[53] M. Mallet, K. Barthélémy, C. Ruby, A. Renard, S. Naille, Journal of Colloid and Interface Science 407 (2013) 95-101.
[54] X. Wang, W. Li, R. Harrington, F. Liu, J.B. Parise, X. Feng, D.L. Sparks, Environmental Science & Technology 47 (2013) 10322-10331.
[55] Z. Ajmal, A. Muhmood, M. Usman, S. Kizito, J. Lu, R. Dong, S. Wu, Journal of Colloid and Interface Science 528 (2018) 145-155.
[56] J.T.N. Knijnenburg, K. Laohhasurayotin, P. Khemthong, W. Kangwansupamonkon, Chemosphere 223 (2019) 310-318.
[57] R.-h. Li, J.-l. Cui, X.-d. Li, X.-y. Li, Environmental Science & Technology 52 (2018) 14119-14128.
[58] S. Fujieda, K. Shinoda, S. Suzuki, Advances in Materials Science for Environmental and Energy Technologies III 250 (2014) 35-41.
[59] J.J. Bravo-Suárez, E.A. Páez-Mozo, S.T. Oyama, Química Nova 27 (2004) 601-614.
[60] E. Kanezaki, Solid State Ionics 106 (1998) 279-284.
[61] L.P. Cardoso, J.B. Valim, Journal of Physics and Chemistry of Solids 67 (2006) 987-993.
[62] J.A. Carrasco, A. Harvey, D. Hanlon, V. Lloret, D. McAteer, R. Sanchis-Gual, A. Hirsch, F. Hauke, G. Abellán, J.N. Coleman, E. Coronado, Chemical Communications 55 (2019) 3315-3318.
[63] K.M.G. Mostofa, C.-q. Liu, M.A. Mottaleb, G. Wan, H. Ogawa, D. Vione, T. Yoshioka, F. Wu, in: K.M.G. Mostofa, T. Yoshioka, A. Mottaleb, D. Vione (Eds.), Photobiogeochemistry of Organic Matter: Principles and Practices in Water Environments, Springer Berlin Heidelberg, Berlin, Heidelberg, 2013, pp. 1-137.
[64] M. Zubair, M. Daud, G. McKay, F. Shehzad, M.A. Al-Harthi, Applied Clay Science 143 (2017) 279-292.
[65] X. Zhang, L. Guo, H. Huang, Y. Jiang, M. Li, Y. Leng, Water Research 96 (2016) 280-291.